ELSEVIER

Journal of Nuclear Materials 307–311 (2002) 357–361

journal of nuclear materials

www.elsevier.com/locate/jnucmat

The performance of Chinese 316L and 316Ti stainless steel irradiated at 300, 400, 500 and 600 °C in HFIR JP-23 test capsule

J. Yu [a,*], D.S. Gelles [b], F.A. Garner [b], M.B. Toloczko [a,b], M.L. Hamilton [b], R.J. Kurtz [b], R.H. Jones [b]

[a] China Institute of Atomic Energy, P.O. Box 275-51, Beijing 102413, China
[b] Pacific Northwest National Laboratory, P.O. Box 999, Richland, WA 99532, USA

Abstract

Shear punch tests, density measurements and microstructure observations are reported for Chinese 316 austenitic stainless steel specimens which were isothermally irradiated at temperatures ranging from 300 to 600 °C to doses between 7 and 9 dpa.

1. Introduction

The fusion energy development program in China requires both fusion reactor technology and materials development. The purpose of the present study is to provide a baseline for further science and technology development in support of fusion reactor technology and materials science. Austenitic stainless steels have been developed and have widely been used in the nuclear industry. Therefore, this steel is a prime candidate for the first fusion reactor in China. 316L and 316Ti modified stainless steel manufactured in China have been irradiation to 50 dpa with alpha particles and proton irradiation [1,2]. The present work examines the performance of these materials following irradiated by neutrons. Chinese 316L and 316Ti stainless steels specimens were irradiated in the high flux isotope reactor (HFIR) in HFIR-MFE-200J-1, HFIR-MFE-400J-1, HFIR-JP-20, HFIR-JP-21, HFIR-JP-22, HFIR-JP-23 test capsules at Oak Ridge National Laboratory (ORNL). Specimen conditions included solution-annealed (SA) and 20% cold-worked, and irradiations were at 300, 400, 500 and 600 °C to 9.04 dpa in the HFIR-JP-23 test capsule. Following irradiation, specimen microstructures were studied using transmission electron microscopy (TEM) as well as density measurements and hardening was determined using shear punch testing. The mean He/dpa for various irradiation temperatures were between 38.9 and 45.8 appm He/dpa [3,4].

2. Experimental

2.1. Specimens and irradiation conditions

The chemical compositions of the specimens used are given in Table 1. The C316L and C316Ti specimens were SA at 1050 °C for one hour (C316L-SA) and a half hour (C316Ti-SA), respectively, or were cold-rolled ~20% after solution-annealing (C316L-20%CW, C316Ti-20%CW).

The specimens were irradiated in the HFIR-JP-23 capsule. The maximum neutron fluence at midplane for the JP-23 capsule was about 4.39×10^{22} n/cm^2 and the fast neutron fluence was about 1.13×10^{22} n/cm^2 ($E >$ 0.1 MeV) corresponding to 9.04 dpa in type 316 stainless

* Corresponding author. Tel.: +86-10 693 57232; fax: +86-10 693 57008.
E-mail address: yujn@iris.ciae.ac.cn (J. Yu).

0022-3115/02/$ - see front matter © 2002 Elsevier Science B.V. All rights reserved.
PII: S0022-3115(02)01138-8

Table 1
Chemical compositions for Chinese 316L and 316Ti (wt%) (balance Fe)

	C	Si	Mn	Ni	P	S	Cr	Mo	Co	Ti	B	N
C316L	0.025	0.29	1.41	14.14	0.017	0.015	17.22	2.25				
C316Ti	0.055	0.80	1.79	13.47	0.022	0.029	17.9	2.64	0.033	0.319	0.0013	0.032

steel [3]. All JP-23 capsules used gas-gapped holders designed to operate at irradiation temperatures of 300, 400, 500 and 600 °C [4]. Dependent on the distance from the midplane for each TEM specimen holders, the irradiation doses (dpa) of specimens at irradiation temperatures of 300, 400, 500 and 600 °C were 6.8, 7.9, 8.6 and 9.0, respectively. The corresponding He/dpa ratios for the various irradiation temperatures were 38.9, 42.3, 44.6 and 45.7 appm/dpa [3].

2.2. Mechanical test and swelling measurements

Shear punch tests were performed at room temperature on unirradiated control specimens and the irradiated TEM disks of C316 austenitic stainless steel using the standard fixture in service from 1996 at PNNL [5,6]. Reference specimens were tested prior to performing tests on the controlled and irradiated specimens. Data were analyzed electronically using a National Instruments DAQ board and LabView software. Shear yield stress was measured at deviation from linear loading, and shear ultimate stress was measured at maximum load. Uniaxial yield stress, ultimate stress, and uniform elongation were predicted from correlations established by Hankin et al. [5,6]. Irradiation induced swelling was determined by comparison of pre- and post-irradiation immersion density measurements. Typically three to five measurements were made on each specimen, giving a 3σ uncertainty of 0.15%.

2.3. Microstructural observations

Specimens for TEM were thinned on a Struer's Tenupol twin-jet electropolishing apparatus using an electrolyte of 10% perchloric acid in methanol operating at −20 °C at 50 V and 1 mA in a shielded hood. TEM disks were examined using a JEOL JEM-1200 transmission electron microscope operated at 120 keV and equipped with a double-tilting goniometer stage. The foil thicknesses for the analysis areas were measured based on stereo methods in order to quantify defect densities.

3. Results and discussion

3.1. Mechanical properties

The results of measured shear yield stress and shear ultimate stress are shown in Table 2. The true uniform elongation values are within the range observed for miniature tensile tests on SA and 20% cold-worked 316 SS [5,7]. However, the results indicate that: (1) The uniaxial yield strength from the shear punch tests is consistent with tensile data in the literature [8] in the same range of irradiation temperature. (2) The ultimate strength is higher than that reported in the literature [9,10], but this may be due to the fact that most tensile tests were performed at the irradiation temperature. (3) The true uniform elongation is high for the 300 and 600 °C irradiation temperatures [8], but is consist with the results at 400 and 500 °C [9]. (4) The uniaxial yield stress at 400 °C was slightly greater than at 300 °C, and above 400 °C, the uniaxial yield stress decreased with increasing temperature. This is because the radiation induced structure scale (depleted zones and dislocation loop spacing) increased with increasing temperature. (5) The ultimate strength was nearly constant for the irradiation temperatures from 300 to 500 °C, and then decreased for the 600 °C irradiation temperature. (6) All conditions

Table 2
The mechanical properties of C316 stainless steel irradiated at various temperatures

Matr.	C316L-SA			C316L20%CW			C316Ti-SA			C316Ti20%CW		
Unirr.	σ_y (MPa)	σ_s (MPa)	δ (ε_u) (%)	σ_y (MPa)	σ_s (MPa)	δ (ε_u) (%)	σ_y (MPa)	σ_s (MPa)	δ (ε_u) (%)	σ_y (MPa)	σ_s (MPa)	δ (ε_u) (%)
	268	700	35.8	598	679	9.8	177	608	40.6	712	834	10.4
300 °C (∼7 dpa)	829	931	8.1	642[a]	855[a]	14.8	873	1064	10.9	1016	1083	5.0
400 °C (∼8 dpa)	741	855	9.2	719	808	8.4	917	1026	7.3	1027	1100	5.9
500 °C (∼8.5 dpa)	675	792	10.4	741	817	7.8	NA[b]	NA[b]	NA[b]	785	1022	14.0
600 °C (∼9 dpa)	334	680	28.8	521	756	18.5	345	813	34.2	609	889	18.5

[a] Specimen could not be positively identified.
[b] Bad specimen due to large thickness gradient.

appear to undergo radiation softening at 600 °C irradiation temperature, i.e. the yield stress and ultimate strength decrease and the uniform elongation increases. Therefore, softening occurs at the 600 °C irradiation temperature.

3.2. Density measurement

Density measurements were performed at room temperature on the unirradiated control specimens and the irradiated TEM disks of C316 austenitic stainless steel. The density change for all irradiated specimens was densification in the range 0.5–2%. Densification is usually a result of precipitation during irradiation.

3.3. Microstructural evolution

The TEM observation results are summarized in Table 3. Microstructures of the alloys (C316L-SA, C316L-20%CW, C316Ti-SA and C316Ti-20%CW) irradiated at 300 °C to 6.86 dpa with 267 appm transmuted helium from the HFIR-JP-23 capsule are shown in Fig. 1. Small cavities (or bubbles) were observed with mean size of ~2 nm and number densities at $\sim 2\text{–}10 \times 10^{21}$ m^{-3}. The transmuted He and H may induce these high cavity (or bubble) densities at 300 °C. The corresponding dislocation loop densities were about 0.73–2.10×10^{15} m^{-2} and the loop mean size was about 11 nm. Brager and Garner indicated that void densities generated in HFIR saturate at less than 7 dpa and before 300 appm of helium can accumulate [11]. New Russian data continue to show swelling at temperatures above 305 °C in various stainless steels [12]. The irradiation temperature of specimens in HFIR-JP-23 may be between 300 and 325 °C [4,11] and observation of cavities is reasonable.

The mean size of cavities increases with the irradiation temperature to 600 °C. The cavity density was highest for irradiation at 400 °C, and therefore lower at 300 °C, whereas above 400 °C, it decreased with increasing temperature. Because the irradiation dose and He/dpa ratio for specimens irradiated at 400 °C were higher than that at 300 °C, the cavity density for specimens irradiated at 400 °C is higher than that for 300 °C irradiated specimens. At irradiation temperatures from 400 to 600 °C, the cavity coalescence becomes important, decreasing cavity densities.

The swelling increases with the irradiation temperature from 300 to 600 °C as shown in Table 3. There is no significant difference in the incubation period for swelling between SA and 20% cold-worked conditions. However, swelling from cavitation is too small to induce a macro-density change. When the irradiated temperature was higher than 500 °C, a bi-modal size distribution of voids developed, as shown in Fig. 2. The bi-modal distribution indicates mixed populations of smaller sub-critical

Table 3
Microstructure observation data of C316 stainless steel irradiated at various temperatures

	C316L-SA				C316L20%CW				C316Ti-SA				C316TI20%CW			
Irr. Temp.	300	400	500	600	300	400	500	600	300	400	500	600	300	400	500	600
Doses (dpa)	7	8	8.5	9	7	8	8.5	9	7	8	8.5	9	7	8	8.5	9
C_v (10^{16} cm^{-3})	0.17	2.69	0.49	0.97	0.88	22.70	2.59	0.70	0.27	1.70	0.70	0.88	1.20	0.68	1.09	5.77
D_v (nm)	2.13	3.04	6.13	6.51	1.58	2.26	3.35	7.54	1.21	2.77	5.29	3.73	2.69	3.24	2.93	5.57
S (%)	0.001	0.04	0.10	0.48	0.002	0.13	0.11	0.53	~0	0.007	0.08	0.03	0.002	0.04	0.10	0.49
C_d (10^{16} cm^{-3})	0.23	1.72	0.32	0.87	6.67	3.97	114.0	8.83	2.06	3.63	1.33	0.29	2.72	0.71	0.80	0.44
D_d (nm)	11.63	11.40	17.79	13.45	10.03	13.05	19.23	38.42	11.41	11.32	17.27	31.18	5.50	7.41	18.14	25.31
$\pi D_d C_d$ (10^{11} cm^{-2})	0.09	0.62	0.18	0.37	2.10	1.63	68.86	10.66	0.74	1.29	0.72	0.28	1.32	0. 38	0.46	0.35

C_v – Concentration of voids, D_v – mean diameter of voids, S – swelling, C_d – number density of dislocation loop, D_d – mean diameter of dislocation loop.

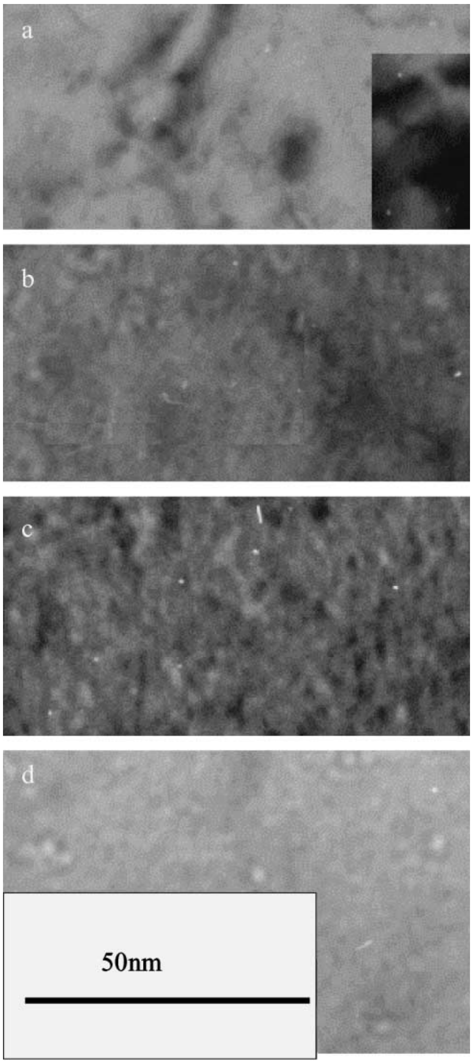

Fig. 1. The small voids in C316 SS specimens irradiated at 300 °C to ~7 dpa, (a) C316L SS SA, (b) C316L SS-20%CW, (c) C316Ti SS SA and (d) C316TiSS-20%CW (bright field images).

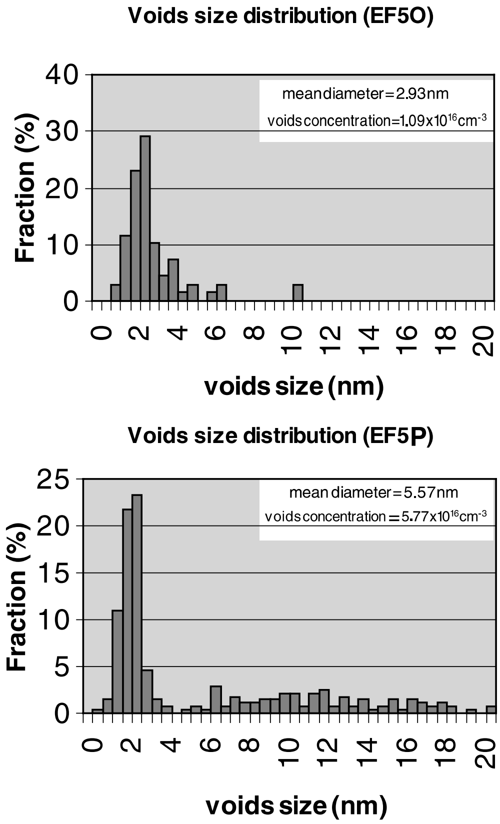

Fig. 2. The size distribution of voids in C316Ti SS-20%CW irradiated at 500 °C to ~8.5 dpa (EF5O) and at 600 °C to ~9 dpa (EF5P).

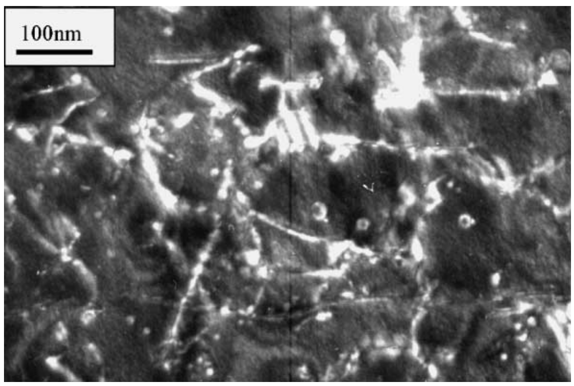

Fig. 3. The voids pinned at dislocations in 316L SS-20%CW irradiated at 600 °C to ~9 dpa (dark field image).

helium bubbles and larger bias-driven voids. Fig. 3 shows that most of the small voids (or bubbles) were pinned at dislocation and dislocation loop and the large voids were mostly unpinned. Small voids (or bubbles) pinned at dislocations and dislocation-loops grow slowly because of the preferential absorption of interstitial atoms at dislocations. The larger bias-driven voids in the matrix have evolved to larger sizes forming the bi-modal distribution.

3.4. Dislocation loop evolution

Fig. 4 shows dislocation loops in the C316L-SA stainless steel irradiated at 400 °C to 8 dpa. The image was taken with beam direction close to [0 1 1] using $g = \langle 200 \rangle$ in bright-field contrast. The Frank-type faulted loops appear on $\{111\}$ planes, identified by stacking faults in weak beam dark-field images. The dislocation loop data in the alloys are summarized in Table 3. The mean size of dislocation loops increased

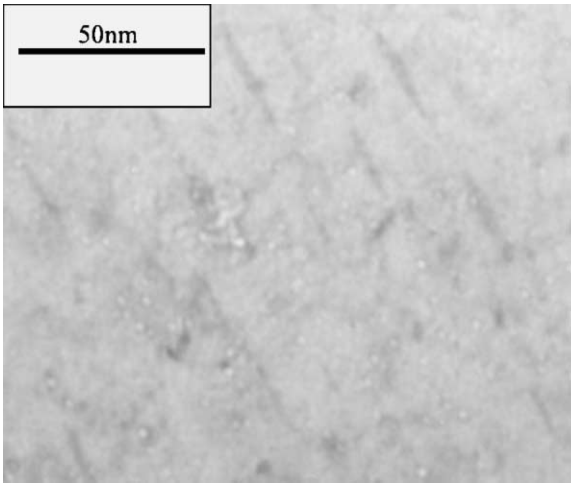

Fig. 4. Faulted frank loops on {1 1 1} planes in the C316L-SA stainless steel irradiated at 400 °C to 8 dpa (bright-field image).

with the irradiation temperature. The number density of dislocation loops for the SA condition was greatest at 400 °C, and above 400 °C, the number density of dislocation loops decreased with increasing temperature. But the loop number density for the 20% cold-worked condition first decreased from 300 to 400 °C and increased from 400 to 600 °C.

3.5. Precipitate evolution

Some carbide precipitates ($M_{23}C_6$) were often observed. The larger ones were mostly on grain boundaries. Although the γ' phase ($Ni_3(Ti,Si)$) was sometime observed in specimens of 316Ti stainless steel irradiated at 400 and 500 °C, they were too small to discriminate from small carbides and Frank loops. This is because the irradiation fluence and Si content in Chinese 316Ti SS specimens are not large enough to form observable γ' phase.

4. Summary

Shear punch tests, density measurements and microstructure observation were performed at room temperature on TEM disks C316 austenitic stainless steel irradiated at temperatures from 300 to 600 °C to doses between 7 and 9 dpa.

(1) The uniaxial yield stress at 400 °C was slightly greater than at 300 °C, whereas above 400 °C the uniaxial yield stress decreased with increasing temperature.
(2) The ultimate strength was nearly constant for the irradiation temperatures from 300 to 500 °C, and then decreased for the 600 °C irradiation temperature. The yield stress and ultimate strength decreased and uniform elongation increased to show the grain softening at the 600 °C irradiation temperature.
(3) Density measurements of the irradiated specimens showed densification of 0.5–2% for all conditions, with the exception of C316Ti-SA at 400 and 600 °C.
(4) Small cavities (or bubbles) were observed in all specimens irradiated at 300 °C to 6.8 dpa. The mean size was about 2 nm and the number densities were about $2\text{–}10 \times 10^{21}$ m^{-3}.
(5) A bi-modal size distribution of voids occurs at irradiation temperatures higher than 500 °C. Most of small voids (or bubble) are pinned at dislocations and dislocation loops whereas the large voids were mostly independent.

Acknowledgements

This work was supported by US Department of Energy (DOE) under the US – PRC Program of Co-operation.

References

[1] J. Yu, X. Zhao, W. Zhang, et al., J. Nucl. Mater. 251 (1997) 150.
[2] J. Yu, Y. Chen, Q. Yang, et al., J. Nucl. Mater. 191–194 (1992) 728.
[3] L.R. Greenwood, R.T. Ratner, Neutron dosimetry and damage calculations for the HFIR-JP-23 irradiations, Fusion Reactor Materials Semiannual Progress Report, DOE/ER-0313/20, 1996, p. 305.
[4] A.M. Ermi, D.S. Gelles, Preliminary Report on the Irradiation Conditions of the HIFR JP-23 Experiment, Fusion Reactor Materials Semiannual Progress Report, DOE/ER-0313/17, 1995, p. 35.
[5] M.L. Hamilton, F.A. Garner, G.L. Hankin, R.G. Faulkner, M.B. Toloczko, ASTM STP 1366 (2000) 1003.
[6] G.L. Hankin, M.B. Toloczko, M.L. Hamilton, R.G. Faulkner, J. Nucl. Mater. 258–263 (1998) 1651.
[7] M.B. Toloczko, M.L. Hamilton, G.E. Lucas, J. Nucl. Mater. 283–287 (2000) 987.
[8] G.E. Lucas, M. Billone, J.E. Pawel, M.L. Hamilton, J. Nucl. Mater. 233–237 (1996) 207.
[9] M.L. Grossbeck, P.J. Maziasz, J. Nucl. Mater. 85&86 (1979) 883.
[10] J.E. Pawel, A.F. Rowcliffe, D.J. Alexander, M.L. Grossbeck, K. Shiba, J. Nucl. Mater. 233–237 (1996) 202.
[11] H.R. Brager, F.A. Garner, The microchemical evolution and swelling of AISI 316 irradiated in HFIR and EBR-II, Dimensional stability and mechanical behaviour of irradiated metals and alloys, British Nuclear Energy Society, London, 1984.
[12] F.A. Garner, A new materials issue for license extension of pressurized water reactors: void swelling and its associated embrittlement, Lecture in China Institute of Atomic Energy, 30 October 2000.